

Tests on the Vibro-Acoustic Behaviour of a Brushless DC-Motor

W. Heylen, W. Desmet, R. Belmans

Abstract

In the design of rotating electrical machines, the vibro-acoustic behaviour becomes an important criterion. In an electrical machine, electromagnetically induced forces may cause vibrations of, for instance, the stator. These vibrations may radiate annoying acoustic energy, especially at resonances of the stator assembly. This paper describes some techniques to analyse the vibro-acoustic behaviour of a (brushless DC-) motor. However, the technique is quite general and can be used for all types of electrical machines. The “inverse-frequency-response-function” technique (IFRF) allows the identification of the actual vibration behaviour of the motor frame from the measurement of the acoustic field around the motor. Experimental modal analysis yields the resonant behaviour of the motor. A combination of both techniques indicates the critical resonances, causing the undesired acoustic emissions. This may lead to an improved, quieter design of the electrical motor.

1 Introduction

The importance of the vibro-acoustic behaviour of rotating electrical machines in particular is steadily growing. The acoustic energy radiated by an electrical motor has become a key item in the design towards more comfortable machinery. Customer demands regarding acoustic emission are getting more and more pronounced as electrical motors are entering applications in silent surroundings such as air conditioning, office equipment and elevators. The mechanical vibrations of an electrical motor may not only cause fatigue and breakdown of the machine, but they may also have a significant contribution to the radiated acoustic noise. This paper focuses on the relation between the motor frame vibrations and the acoustic emission.

The vibro-acoustic behaviour of a motor strongly depends on the frequency content of the electromagnetically induced forces. In this respect, the frequency content of a brushless DC-motor exhibits some characteristic features. First of all, the permanent-magnet excitation, and especially the rectangular or trapezoidal flux density distribution in the air-gap of a brushless DC-motor generated by the permanent magnets, is causing additional force components not found in, for instance, induction motors. The rectangular current shape, impressed to the motor by the inverter to control the speed and to position the motor when used in servo drives, is a second cause of additional force components.

As a high acoustic noise level can be expected when a force component frequency matches a resonance frequency of the stator, the knowledge of these dynamic quantities is essential. A correct analysis of the force components is difficult and involves advanced electromagnetic field calculation techniques, based on the finite element method [1–3], to take into account the non-linear behaviour of the iron. Due to the composite nature of the stator assembly (the windings are linked to the stator iron by the electrical insulation material,

while the stator laminations are pressed in the stator frame), an experimental rather than a theoretical approach is preferred since the material parameters are difficult to assess.

In order to show the present possibilities found in mechanical engineering, this paper compares some experimental techniques for describing the vibro-acoustic behaviour of electrical motors. Acoustic techniques such as “near-field acoustic holography” [4] and “inverse frequency-response-function (IFRF) methods” [5] allow identifying acoustic sources from near-field pressure measurements. Experimental modal analysis [6] determines the resonance frequencies and corresponding deformation patterns from input (force) and output (structural displacement, velocity or acceleration) measurements. The reported tests concentrate on the acoustic emission caused by the motor frame vibrations only. The acoustic emission caused by other electromagnetic phenomena as e. g. the acoustic noise of the inverter, generated by magnetostriction of ferromagnetic parts, is disregarded. Due to the relatively low flux density levels used in rotating machines when compared to e. g. coils and transformers, magnetostriction is usually negligible in such devices.

2 Experimental Set-Up

The tests have been performed on an brushless DC-motor ($T_n = 3.2$ Nm, $I_n = 5.9$ A, $U_n = 260$ V). The rotor has Samarium-Cobalt permanent magnets. **Fig. 1** gives a schematic view on the experimental set-up. The brushless DC-motor is suspended on a frame. The force input for the experimental modal analysis is measured using a load cell mounted on an excitation hammer. The vibration response of the motor frame may be measured with accelerometers or a laser-Doppler vibrometer. The latter is used here, measuring the structural velocity by pointing the laser beam at various positions on the motor

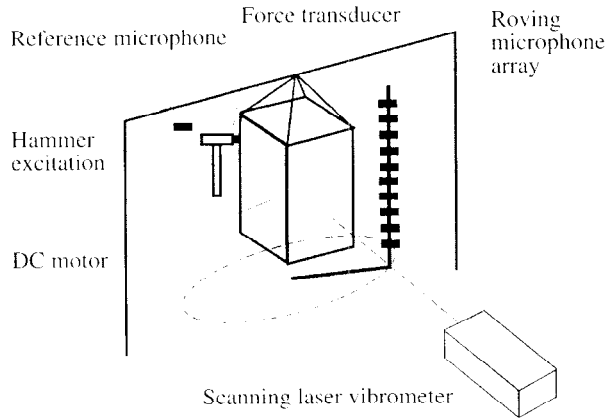


Fig. 1. Experimental set-up

frame surface. Since this measurement is contactless, it has no influence on the vibrations of the motor frame and it is less sensitive to heat or magnetic fields. This is particularly important, as the response to be analysed here is very small and would be disturbed by attaching accelerometers to the motor frame surface. The acoustic measurements are carried out by roving a linear array of ten microphones on 24 equidistant angular positions on a cylindrical surface around the motor. Cross-spectral density measurements with a fixed reference microphone are used to phase lock the measurements of the 24 array positions relative to each other.

A first set of measurements determines the most important frequencies in the acoustic spectrum of the motor, by varying the motor speed from 3000 min^{-1} (50 Hz) to standstill. In the frequency range up to about 2000 Hz, two frequency ranges are found with major acoustic noise levels: one around 850 Hz and one around 1600 Hz. These preliminary measurements justify concentrating further measurements around these two frequency values. Higher noise levels are detected also in the 4.5 kHz to 7 kHz range. These are probably caused by other electromagnetic phenomena as e. g. the acoustic noise of the inverter, caused by magnetostriction of ferromagnetic parts.

3 Acoustic Measurements

For the identification of acoustic sources from acoustic pressure measurements, two techniques can be applied: the near-field acoustic holography technique and the inverse FRF technique. Near-field acoustic holography allows the reconstruction of the sound pressure distribution in a three-dimensional space from the measurement of sound pressures in a two-dimensional plane. The inverse FRF technique yields the identification of the strengths of acoustic sources at some known locations from an array of sound pressure measurements. The latter technique has been adopted in the tests.

The inverse FRF technique starts from a matrix equation, relating a $(n_i \times I)$ vector of strengths Q_i of acoustic sources at n_i known locations to a $(n_r \times I)$ vector of sound pressures p_r at n_r known response locations. In the frequency domain, this equation is:

$$\{p_r(f)\} = [\mathbf{H}(f)]\{Q_i(f)\}, \quad (1)$$

where $[\mathbf{H}(f)]$ is a $(n_r \times n_i)$ frequency response function (FRF) matrix.

If the FRF matrix $[\mathbf{H}(f)]$ is known, the source strength vector $\{Q_i(f)\}$ can be estimated from the measured response pressures $\{p_r(f)\}$ as follows:

$$\{Q_i(f)\} = [\mathbf{H}(f)]^+ \{p_r(f)\}, \quad (2)$$

where $[\mathbf{H}(f)]^+$ is the pseudo-inverse of $[\mathbf{H}(f)]$.

The aim of the present study is to identify the main acoustic noise radiating parts of a rotating electrical machine. In this case, the mechanical vibrations of the motor frame may be regarded as a continuous distribution of acoustic sources, rather than a collection of point sources at some discrete locations. In such a case, the FRF matrix $[\mathbf{H}(f)]$ in eq. (1) can be identified in an experimental or a numerical way.

3.1 Experimental Identification of the FRF Matrix

Structure-borne acoustic noise results from the vibrations of a mechanical structure. As shown in Fig. 2, a vibrating structure with surface S may be regarded as a continuous distribution of acoustic volume velocity sources. Each source has an infinitesimally small surface area dS and a source strength $Q(\mathbf{r}_S, f) = v_n(\mathbf{r}_S, f) dS$, where $v_n(\mathbf{r}_S, f)$ is the normal structural velocity component with frequency f at position \mathbf{r}_S at the structural surface S . This continuous source distribution may be approximated as a collection of n_i finite-sized sources with surface area ΔS_i and source strength $Q_i(f) = v_{ni}(f) \Delta S_i$, where $v_{ni}(f)$ is the averaged surface normal velocity. Provided that the dimensions of the surface areas are substantially smaller than the structural and acoustic wavelengths at the considered frequency, the total sound pressure $p_r(f)$ at a certain response position r may be approximated as:

$$\begin{aligned} p_r(f) &= \int_S \left[\frac{p_r(f)}{Q(\mathbf{r}_S, f)} \right] v_n(\mathbf{r}_S, f) dS(\mathbf{r}_S) \\ &\approx \sum_{i=1}^{n_i} \left[\frac{p_r(f)}{Q_i(f)} \right] v_{ni}(f) \Delta S_i \\ &= \sum_{i=1}^{n_i} H_{ri}(f) Q_i(f). \end{aligned} \quad (3)$$

Each frequency response function $H_{ri}(f) = p_r(f) / Q_i(f)$ in eq. (3) relates the sound pressure at response location r to the strength of an acoustic source excitation

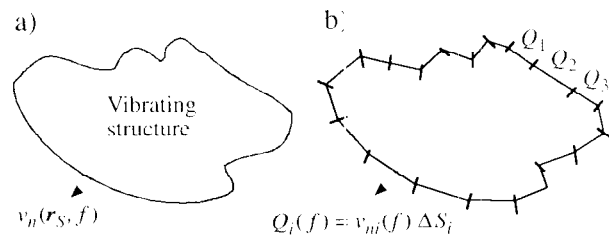


Fig. 2. Vibrating structure
a) Geometrical view
b) Approximate source description

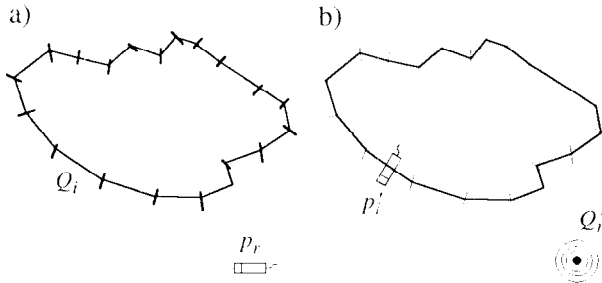


Fig. 3. FRF measurements
a) Direct measurement
b) Reciprocal measurement

at location i . All these FRFs of the $(n_r \times n_i)$ matrix $[\mathbf{H}(f)]$ in eq. (1) can be identified in an experimental way [7, 8]. Since it is usually very difficult or even impossible to practically induce some vibrations on a part ΔS_i of the structure, while keeping all other parts undeformed, the experimental identification of the FRFs is commonly based on the acoustic reciprocity relation:

$$H_{ri}(f) = \left[\frac{p_r(f)}{Q_i(f)} \right] = \left[\frac{p'_i(f)}{Q'_r(f)} \right]. \quad (4)$$

As illustrated in **Fig. 3**, this reciprocity relation indicates that the relation between the sound pressure p_r at response location r and the strength Q_i of an acoustic source excitation at location i can be obtained by measuring the sound pressure p'_i at the original source location i due to an omni-directional acoustic source excitation Q'_r at the original response location r . Note that, during this measurement, the original excitation, causing the structural vibrations, must be turned off.

3.2 Numerical Identification of the FRF Matrix

The numerical identification of the FRF matrix may be based on the direct boundary integral formulation for exterior acoustic problems [9]. This formulation states that the sound pressure $p(\mathbf{r}, f)$ at any position \mathbf{r} in an acoustic domain, exterior to a vibrating structure with a closed surface S , can be expressed as

$$p(\mathbf{r}, f) = \int_S \left[p(\mathbf{r}_S, f) \frac{\partial G(\mathbf{r}, \mathbf{r}_S, f)}{\partial n} + j 2\pi f \rho v_n(\mathbf{r}_S, f) G(\mathbf{r}, \mathbf{r}_S, f) \right] dS(\mathbf{r}_S), \quad (5)$$

where $p(\mathbf{r}_S, f)$ and $v_n(\mathbf{r}_S, f)$ are, respectively, the pressure and normal structural velocity components with frequency f at each position \mathbf{r}_S on the structural surface S , ρ the mass density of the fluid in the acoustic domain and n the direction, normal to the surface. The Green's kernel function $G(\mathbf{r}, \mathbf{r}_S, f)$ represents the free-field pressure at position \mathbf{r} due to an acoustic point source excitation at position \mathbf{r}_S ,

$$G(\mathbf{r}, \mathbf{r}_S, f) = \frac{e^{-j \frac{2\pi f}{c} |\mathbf{r} - \mathbf{r}_S|}}{4\pi |\mathbf{r} - \mathbf{r}_S|}, \quad (6)$$

where c is the speed of sound in the fluid.

The direct boundary element method (BEM) [10] provides a numerical way to assess the sound pressure field due to a vibrating structure. As can be seen from eq. (5), this pressure field is completely defined, once the pressure distribution $p(\mathbf{r}_S, f)$ and the normal velocity distribution $v_n(\mathbf{r}_S, f)$ at the closed surface S are known. In the BEM, the numerical approximation of these distributions results from discretizing the surface S into some small, usually triangular or quadrilateral, boundary elements. In each element, some nodes are defined, usually at the element corner positions. Assuming that the surface element discretization has a total of n_i nodes and that the dimensions of each boundary element are substantially smaller than the structural and acoustic wavelengths at the considered frequency, the surface distributions $p(\mathbf{r}_S, f)$ and $v_n(\mathbf{r}_S, f)$ may be approximated as:

$$p(\mathbf{r}_S, f) \approx \sum_{i=1}^{n_i} N_i(\mathbf{r}_S) p_i(f) = [\mathbf{N}_i(\mathbf{r}_S)] \{p_i(f)\}, \quad (7)$$

$$v_n(\mathbf{r}_S, f) \approx \sum_{i=1}^{n_i} N_i(\mathbf{r}_S) v_{ni}(f) = [\mathbf{N}_i(\mathbf{r}_S)] \{v_{ni}(f)\}. \quad (8)$$

Each nodal shape function $N_i(\mathbf{r}_S)$ in the $(I \times n_i)$ matrix $[\mathbf{N}_i(\mathbf{r}_S)]$ has only a non-zero value in the domains of those elements, to which node i belongs. In these element domains, the shape function has a unit value at node position i , it is zero at all other node positions of the element and it has a predefined, usually linear shape in-between the element nodes. In all other boundary element domains, the shape function is identically zero. The $(n_i \times I)$ vectors $\{p_i(f)\}$ and $\{v_{ni}(f)\}$ contain, respectively, the pressure and normal velocity approximations at the node positions (**Fig. 4**).

The substitution of the approximations (7) and (8) and the Green's kernel function (6) into the integral formulation (5) yields an approximation of the $(n_r \times I)$ vector of sound pressures p_r at n_r response locations

$$\{p_r(f)\} \approx [\mathbf{D}(f)] \{p_i(f)\} + [\mathbf{E}(f)] \{v_{ni}(f)\}, \quad (9)$$

where the elements of the $(n_r \times n_i)$ matrices $[\mathbf{D}(f)]$ and $[\mathbf{E}(f)]$ result from some numerical integrations.

A slightly modified version of the direct boundary integral formulation enables to relate the sound pressure $p(\mathbf{r}, f)$ at a position \mathbf{r} on the closed surface S of the vibrating structure to the pressure and normal velocity distribution on this boundary surface,

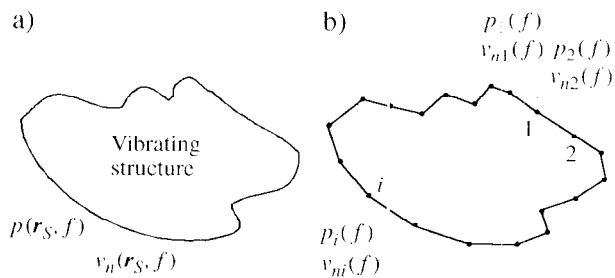


Fig. 4. Pressure and normal velocity distributions
a) Vibrating structure
b) Boundary element discretization

$$C(\mathbf{r}) p(\mathbf{r}, f) = \int_S \left[p(\mathbf{r}_S, f) \frac{\partial G(\mathbf{r}, \mathbf{r}_S, f)}{\partial n} + j 2\pi f \rho v_n(\mathbf{r}_S, f) G(\mathbf{r}, \mathbf{r}_S, f) \right] \cdot dS(\mathbf{r}_S). \quad (10)$$

The coefficient $C(\mathbf{r})$ depends on the geometrical shape of the vibrating surface S . At surface positions, where the normal direction n is uniquely defined, this coefficient equals 1/2.

By using the approximations (7), (8) and the Green's kernel function (6) for the evaluation of the integral formulation (10) at each surface position \mathbf{r} , coinciding with a node position i of the boundary element discretization, a square matrix equation is obtained, relating the vector of nodal pressures to the vector of nodal normal velocities,

$$[A(f)] \{p_i(f)\} = [B(f)] \{v_{ni}(f)\}. \quad (11)$$

Again, the elements of the $(n_i \times n_i)$ matrices $[A(f)]$ and $[B(f)]$ result from some numerical integrations.

The combination of the matrix eqs. (9) and (11) yields the required matrix equation

$$\{p_r(f)\} = [H(f)] \{v_{ni}(f)\} \quad (12)$$

with the numerically identified FRF matrix:

$$[H(f)] = [D(f)] [A(f)]^{-1} [B(f)] + [E(f)]. \quad (13)$$

Note that the numerical identification of the FRF matrix involves nodal normal velocities, rather than source volume velocities, involved in the experimental identification.

In the present vibro-acoustic study of a brushless DC-motor, the numerical identification procedure is used. For this purpose, a boundary element discretization of 192 nodes and 199 elements is made for the closed surface, coinciding with the exterior surface of the motor.

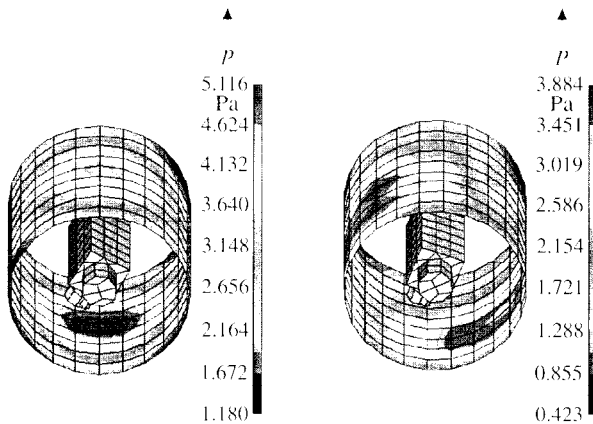


Fig. 5. Measured sound pressures at 855 Hz (left) and 1589 Hz (right)

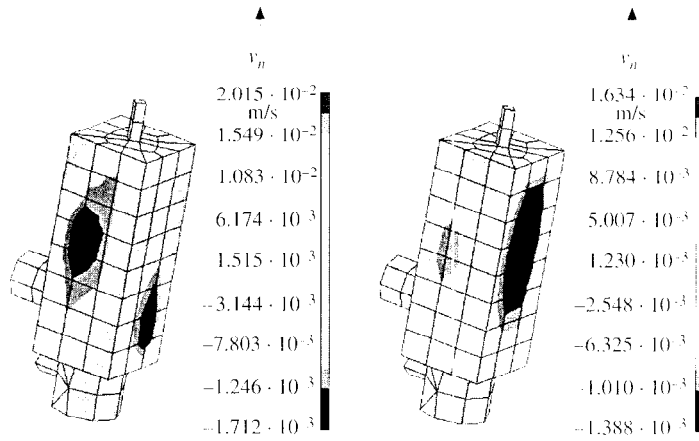


Fig. 6. Normal velocity reconstruction at 855 Hz (left) and 1589 Hz (right)

Fig. 5 shows the measured sound pressure distributions on the cylindrical surface around the motor at the two frequencies of major acoustic emission (see Section 2).

The application of the inverse FRF technique, using these measured pressure distributions and the numerically identified FRF matrix (eq. (13)), yields the reconstructed normal velocity distributions at the motor surface (Fig. 6).

From these reconstructed velocity distributions – resulting from some straightforward pressure measurements and from a numerical FRF matrix identification – it can be clearly seen that the high acoustic emissions around 855 Hz and 1589 Hz are mainly caused by substantial vibration levels of the motor frame side walls.

4 Modal Analysis Measurements

Experimental modal analysis [6] is a technique, enabling the determination of the modal parameters (resonance frequencies, damping ratios and modal deformation patterns) of a dynamic system. A dynamic force is applied to the system. The input force and the response of the system at the points of interest are measured. These measurements yield the necessary frequency response functions between the output(s) and the input(s). Since these frequency responses depend on the modal parameters, the latter can be found using a parameter estimation algorithm.

As already mentioned in Section 2, the dynamic force input for a modal test of the considered electrical motor is obtained using an impact hammer. A force transducer, built-in at the tip of the hammer, measures the input force. A laser-Doppler vibrometer is used to assess the velocity of the motor frame. In this case study, only the structural velocities perpendicular to the four side walls of the motor frame are measured. Note that the electrical motor is turned off during these measurements.

Fig. 7 shows a typical measured frequency response function. The peaks around 890 Hz and 1660 Hz are clear indications of structural resonances of the motor

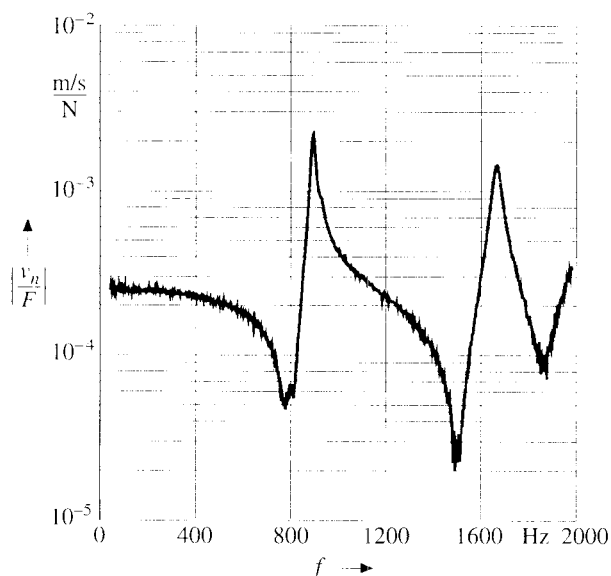


Fig. 7. Typical frequency response function, with resonance peaks at 893 Hz and 1661 Hz

frame. Fig. 8 shows the corresponding mode shapes (only the central area of each motor frame side wall is shown).

These modal analysis results clearly indicate that the strongly radiating vibration patterns of the motor frame, which have been identified from operational acoustic measurements and the application of the inverse FRF technique, are induced by structural resonances of the motor frame. Note, however, that the experimentally identified resonance frequencies (893 Hz, 1661 Hz) slightly differ from the frequencies of high acoustic emission (855 Hz, 1589 Hz). This may be due to the fact that the modal analysis is carried out when the motor is turned off. The fundamental reason of this difference may be found in the higher temperature of the windings carrying current during operation. The current and the flux yield losses and the higher temperature reduces the stiffness of, for instance, the electrical insulation material between conductors and iron laminations. Therefore, resonances of a rotating motor are generally somewhat lower than the resonances of a turned-off motor.

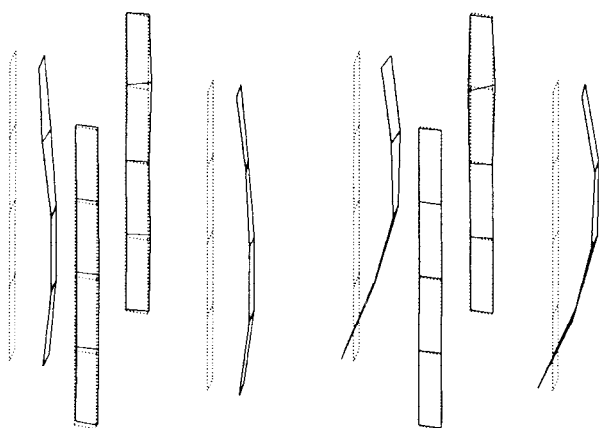


Fig. 8. Mode shapes at 893 Hz (left) and 1661 Hz (right)

5 Conclusions

This paper presents a combined experimental/numerical approach for relating some of the major frequency components in the acoustic emission of a rotating electrical machine to the vibration behaviour of the motor frame. Operational sound pressure measurements indicate the important frequencies of the acoustic emission. A more precise scanning of the sound field around the motor, and the application of the inverse FRF technique, allow the reconstruction of the motor frame normal velocity distributions at these frequencies. A modal analysis experiment on the motor indicates that the frequencies of high acoustic emission correspond to resonance frequencies of the motor frame.

The presented case study illustrates that a combination of acoustic and vibration analysis techniques may provide the necessary insights for an improved, quieter design of an electrical motor.

6 List of Symbols and Abbreviations

6.1 Symbols

c	speed of sound
f	frequency
F	input force
i	source location
n	direction normal to the surface
p	sound pressure
Q	volume velocity
r	response location
ρ	fluid density
S	surface area
v_n	normal velocity

6.2 Abbreviations

BEM	boundary element method
DC	direct current
FRF	frequency response function
IFRF	inverse frequency response function

References

- [1] *Belmans, R.; Verdyck, D.; Geysen, W.*: An approach to modelling of magnetically excited forces in electrical machines. *IEEE Trans. on Magn.* 29 (1993) no. 2, pp. 2032–2035
- [2] *Hameyer, K.; Mertens, R.; Pahl, U.; Belmans, R.*: New technique to enhance the accuracy of 2-D/3-D field quantities and forces obtained by standard finite-element solutions. *IEE Proc. Sci. Meas. Technol.* 145 (1998) no. 2, pp. 67–75
- [3] *Binns, K. J.; Lawrenson, P. J.; Trowbridge, C. W.*: The Analytical and Numerical Solution of Electric and Magnetic Fields. Chichester/GB: J. Wiley, 1994
- [4] *Maynard, J. D.; Williams, E. G.; Lee, Y.*: Near-field Acoustic Holography: Theory of Generalized Holography and the Development of NAH. *J. of the Acoustical Soc. of America* 78 (1985) pp. 1395–1413
- [5] *Dumbacher, S. M.; Brown, D. L.*: Source Imaging Using Acoustic Inverse FRF Array Technique. 14th Int. Modal Analysis Conf., Dearborn, Michigan/USA, February 1996, Proc. pp. 1322–1331

- [6] Heylen, W.; Lammens, S.; Sas, P.: Modal Analysis Theory and Testing. PMA K. U. Leuven/Belgium, 1998
- [7] Mason, J. M.; Fahy, F. J.: Application of a reciprocity technique for the determination of the contributions of various regions of a vibrating body to the sound pressure at a receiver point. Proc. Inst. of Acoustics 12 (1990) P. 1, pp. 469-476
- [8] Verheij, J. W.: On the characterization of the acoustical source strength of structural components. Advanced techniques in Applied and Numerical Acoustics. 6. Int. Semin. on Appl. Acoustics (ISAAC 6), Leuven/Belgium 1995, Proc. course note III, 24 pp.
- [9] Schenck, H. A.: Improved integral formulation for acoustic radiation problems. J. of the Acoustical Soc. of America 44, (1968) pp. 41-58
- [10] Brebbia, C. A.; Telles, J. C. F.; Wrobel, L. C.: Boundary Element Techniques: Theory and Applications in Engineering. Berlin/Germany: Springer, 1984

Acknowledgement

The authors are grateful to the Belgian "Fonds voor Wetenschappelijk Onderzoek Vlaanderen" for its financial support of this work.

Manuscript received on March 19, 1999

The Authors



Ronnie J. M. Belmans (1956) received the MS degree in electrical engineering in 1979 and the PhD degree in 1984, both from the Katholieke Universiteit (K.U.) Leuven, Belgium, the Special Doctorate in 1989 and the "Habilitation" in 1993, both from the RWTH, Aachen, Germany. From 1979 to 1985, he was a member of the staff of the K.U. Leuven. Then he became a research fellow of the National Science

foundation. Since 1993, he is a full professor with the K.U. Leuven, teaching electrical machines, variable speed drives and CAD in magnetics. His research interests include electrical energy systems, rational use of electrical energy, power quality, power electronics, electrical machine design (permanent-magnet motors and induction motors), computer-aided engineering, variable speed drives, and vibrations and audible noise in electrical machines. He was the Director of the NATO Advanced Research Workshop on Vibrations and Audible Noise in Alternating Current Machines (Aug. 1986). He was with the Laboratory for Electrical Machines of the RWTH, Aachen, Germany, as a Von Humboldt Fellow (Oct. 1988 to Sept. 1989). From Oct. 1989 to Sept. 1990, he was a visiting associate professor at Mc Master University, Hamilton, Ont., Canada. During the academic year 1995 to 1996 he occupied the Chair at the London University, offered by the

Anglo-Belgian Society. He is treasurer of SEFI (Société pour l'éducation des ingénieurs) and president of the UIE (Union International pour l'Électrotechnologie). Since January 1999, he is visiting professor at Imperial College of Science, Technology and Medicine, London. He is a fellow of the IEE (United Kingdom), senior member of the IEEE (USA), president of the electrical engineering section of the Koninklijke Vlaamse Ingenieursvereniging (kVIV) and a member of the Editorial Board of ETEP. (K.U. Leuven, Dept. ESAT/ELEN, Kardinaal Mercierlaan 94, B-3001 Leuven, Belgium. Phone: +32 16/32-1020, Fax: +32 16/32 1985, E-mail: ronnie.belmans@esat.kuleuven.ac.be)



Ward Heylen (1956) received the MS degree in mechanical engineering in 1979 from the Katholieke Universiteit (K.U.) Leuven, Belgium and in 1980 from the University of Cincinnati, USA. He received a PhD degree in 1987 from the K.U. Leuven. From 1979 to 1980, he was a teaching and research assistant at the University of Cincinnati. From 1980 to 1990, he was research assistant at the division of

Production Engineering, Machine Design and Automation of the K.U. Leuven. In 1990 he became chief engineer and in 1993 assistant professor at the same division. His research interests include structural dynamics in general and experimental modal analysis and dynamic model updating in particular. (K. U. Leuven, Faculty of Engineering, Dept. of Mechanical Engineering, Celestijnenlaan 300B, B-3001 Leuven, Belgium, Phone: +32 16/32-2486, Fax: +32 16/32 2987, E-mail: ward.heylen@mech.kuleuven.ac.be)



Wim Desmet (1969) received the MS degree in mechanical engineering in 1992 and the PhD degree in 1998, both from the Katholieke Universiteit (K.U.) Leuven, Belgium. From 1992 till 1996, he was a junior research fellow of the National Science Foundation. During the summer of 1995, he was a visiting researcher at the Ray W. Herrick Laboratories, Purdue University, USA. From 1996 till 1998, he was

a research assistant of the K.U. Leuven and since 1999, he is a postdoctoral researcher at the Noise and Vibration Research group of the Department of Mechanical Engineering, K.U. Leuven. His research interests include numerical prediction methods for (coupled) vibro-acoustic analysis, vibro-acoustic testing techniques, active noise and vibration control techniques. His teaching activities include mechanical vibrations and numerical prediction methods for vibro-acoustic design. (K. U. Leuven, Faculty of Engineering, Dept. of Mechanical Engineering-Div. P.M.A., Celestijnenlaan 300B, B-3001 Leuven, Belgium, Phone: +32 16/32-2480, Fax: +32 16/32-2987, E-mail: wim.desmet@mech.kuleuven.ac.be)